

Generative Model for Constructing Reaction Path from Initial to Final States

Akihide Hayashi ^{*1}, So Takamoto¹, Ju Li^{2,3}, and Daisuke Okanohara¹

¹Preferred Networks, Inc., Tokyo, Japan.

²Department of Materials Science and Engineering, Massachusetts Institute of Technology, Cambridge, MA 02139, USA

³Department of Nuclear Science and Engineering, Massachusetts Institute of Technology, Cambridge, MA 02139, USA

January 22, 2024

Abstract

Mapping out reaction pathways and their corresponding activation barriers is a significant aspect of molecular simulation. Given their inherent complexity and nonlinearity, even generating an initial guess of these paths remains a challenging problem. Presented in this paper is an innovative approach that utilizes neural networks to generate initial guess for these reaction pathways. The proposed method is initiated by inputting the coordinates of the initial state, followed by progressive alterations to its structure. This iterative process culminates in the generation of the approximate representation of the reaction path and the coordinates of the final state. The application of this method extends to complex reaction pathways illustrated by organic reactions. Training was executed on the Transition1x dataset, an organic reaction pathway dataset. The results revealed generation of reactions that bore substantial similarities with the corresponding test data. The method’s flexibility allows for reactions to be generated either to conform to predetermined conditions or in a randomized manner.

1 Introduction

Enhanced comprehension of chemical reactions through computational methods is continually advancing. Notably, the intersection of machine learning and computational chemistry has recently shown significant potential for exploration of materials.

The progression rate of a chemical reaction is intrinsically tied to its reaction path (RP). It is a recognized fact that the reaction rate for a chemical reaction can be characterized by a parameter known as activation energy. The activation energy, in atomic terms, is congruent with the energy barrier located on the RP. Determining this activation energy involves finding the saddle point, or transition state (TS), along the minimum energy path (MEP) that connects the initial state (IS) and the final state (FS). As a result, a variety of techniques for calculating MEPs have been cultivated so as to better understand and manipulate chemical reactions.

The gradient method, provided a reasonable initial guess for the Minimum Energy Path (MEP), is frequently utilized to locate the MEP. The Nudge Elastic Band (NEB)[1] and String method[2] are the de facto standard in this context. Before machine learning potentials came into prominence, deploying NEB and String methods was computationally demanding, hence often impractical alongside theories capable of addressing chemical reactions, which are also computationally intensive.

However, the recent evolution of Neural Network Potentials (NNP) has changed this scenario. NNPs are capable of rapidly computing chemical reactions, thus facilitating the analysis of reaction paths. This holds true not just for simple, small-molecule reactions, but also for chemical reactions

*ahayashi@preferred.jp

that involve larger, more complex structures and multiple elementary reactions, such as those seen in catalytic processes.

A crucial issue intensifying in importance in recent years is the generation of an effective initial guess. This particularly applies in the realm of organic compound reactions, for constructing a good initial guess would be quite challenging. It’s worth noting that Minimum Energy Paths (MEPs) are often not unique with many exhibiting high transition states (TS) that are not physically plausible. Reaction paths (RPs) are complexly embedded within phase space in a non-linear manner, making the creation of initial guesses that would lead to low-barrier paths via Nudge Elastic Band (NEB) or String optimization a non-trivial task. As a direct consequence, the quality of reaction path analysis is heavily reliant on the provision of a sound initial guess. This intricate nature poses a significant obstacle to the automatization of reaction path discovery. Although there are some frameworks that enable automatic reaction pathway search by focusing on some reactions, there are some types of reactions that are not suitable for any of the frameworks. Consequently, notably in catalysis research, it often necessitates specialists to extensively invest time in experimentation and iterative processes.

Formulating an initial guess for the reaction pathway is not an insurmountable task, as evident from the ability of experts to infer it successfully. Reasonable Reaction Paths (RPs) aren’t entirely unforeseen; they can be classified into certain discernible patterns. Indeed, many chemical reactions are named and categorized. Meanwhile, the majority of unreasonable RPs, involving the breaking of strong chemical bonds, can be instantly identified for their implausibility. This allows experts to scrutinize the reaction pathways efficiently. However, given the high-dimensionality of potential surfaces, they present significant sparsity in the scope of human comprehension. Considering that, it appears feasible to train a machine learning model to apprehend appropriate RPs by harnessing a large array of chemical reaction data. In particular, the use of a generative model for automatic generation of reaction pathways holds strong promise.

Over the past few years, rapid advancements in machine learning have driven significant progress in generative models, particularly within the context of molecular simulation. Numerous machine learning techniques have emerged, with remarkable strides seen in areas such as diffusion models and flow matching. As a result, a wealth of generative models of atomic structures have been proposed for chemical simulation. A prime example of these techniques is the $E(n)$ equivariant normalizing flow[3]. In this model, each atom of a molecule is represented by coordinates drawn from a Gaussian distribution, and a stable molecular structure is achieved through the process of a normalized flow. In contrast, GeoDiff[4] and the Equivariant flow matching[5] method also use the same Gaussian distribution for atom coordinate sampling, but the models learn the formation direction of the molecular structure, differing from the $E(n)$ model by leveraging a diffusion model and flow matching, respectively, to guide the structural modifications. A shared attribute between these methodologies is the use of a generative process. This process is viewed as a transformation, shifting from a distribution devoid of physical interpretation, to one imbued with physical meaning. Similar efforts have been made to generate reaction paths in the Distributional Graphormer (DiG)[6], which, like GeoDiff, is a diffusion model. This model also experiments with generating reaction paths as part of this study. In DiG, a direct line is traced within a Gaussian distribution, enabling the creation of a pathway that smoothly connects two molecular structures. This is achieved by deterministically generating molecular structures from each point along the line. The methodology, titled "Diffusion Methods for Generating Transition Paths" [7], also RPs using a diffusion model. However, this approach diverges by learning and generating a discrete approximation of the entire reaction pathway. There are also initiatives to integrate Kinetic Monte Carlo[8] methodologies with reinforcement learning[9], offering an alternative to the prevailing diffusion model and flow matching techniques.

In a different approach, we have devised a technique to directly derive a pathway from an IS to a FS via an initial guess of the MEP. Our method forgoes the use of a physically meaningless distribution. Instead, it procures the entire reaction path by smoothly navigating within a configuration that holds significance as a molecular structure. Employing this approach, the entire reaction path can be obtained with reduced computational cost compared to existing methodologies. The architecture needed for generating the entire reaction path fundamentally differs from that of a Neural Network Potential (NNP), which relies solely on a single point in the phase space. Instead, it necessitates an architecture that can overview the trajectory within the phase space, in turn demanding different attributes compared to NNPs. For this reason, we have also developed an architectural model suitable for generation tasks. The model developed in this study can construct suitable reaction paths either

from simple instructions or entirely randomly. The proposed model takes the structure of the IS and reaction type labels as inputs. It then gradually alters the structure from the IS, progressing along the reaction path, to simultaneously infer the approximate RP and FS. This process is computationally inexpensive, capable of learning and generating reaction paths from a dataset. Moreover, our method possesses high versatility as it can train generalizable models based on the Transition1x[10] dataset. Remarkably, it can also create reactions for molecules that contain a higher number of atoms compared to those within the dataset, covering complex organic reactions. This achievement represents an innovative approach to manage the intricate degrees of freedom associated with organic molecules. We envisage several future applications for this approach. One possibility is the method’s use in an off-lattice extension of Kinetic Monte Carlo, employing automatic path search. The technique could also entertain a list of desired reactions, presented in the form of molecular skeletons, and automatically explore reactions satisfying this list. Furthermore, it proves handy for researchers who need to interactively generate initial guesses of reaction pathways.

2 Method

2.1 Theory

The pathways from ISs through RPs to FSs are learned. The basis of the proposed approach is to learn the tangent direction of the RP, denoted by \mathbf{t}_{tan} , at each location on the path in order to determine where to go next. However, if only \mathbf{t}_{tan} is learned and generated, it may deviate from the path due to inference or approximation errors. In such a case, the position far from the path is not learned, resulting in a large deviation from the path. In order to solve this problem, the score matching method and the diffusion model learn which direction to move to in order to return to the area where the data actually appear. In the same way, for the learning reaction paths effectively, it is necessary to learn the direction to the reaction path when it deviates to a position outside the actual reaction path. Let \mathbf{t}_{prp} be the direction back to the reaction path. The actual reaction paths of molecules are high-dimensional and very difficult to illustrate. Therefore, the reaction paths are modeled as curves in a two-dimensional space as shown in Figure 1. In Figure 1, the center of the figure indicates an IS. Each of the three curves leaving from IS indicates a different reaction path. Suppose that these three reaction paths can be expressed by the function $\mathbf{x}_{\text{RP},i_{\text{IS}},c,i_{\text{RP}}}(s)$, where s is a scalar parameter with no physical dimension. RP indicates this function represents a reaction pathway. The i_{IS} is the index of the molecular structure of IS. Let c denote the input vector that characterizes the reaction. There can be multiple reaction pathways leaving from an IS that satisfy the condition of c , and i_{RP} denotes the index that indicates the order among them. In this two-dimensional example, there is only one IS, c is one type, and i_{RP} is 1-3. Given the IS structure and condition c as a condition, we define a direction to go. The direction can be defined as the tangent of the reaction path, found at the point where a perpendicular line intersects this path. There is freedom in choosing the reaction path to follow along. Figure 1 is an example of choosing the spatially nearest reaction path among all the reaction paths using Equation 1.

$$(\hat{s}(i_{\text{IS}}, c, \mathbf{x}), \hat{i}(i_{\text{IS}}, c, \mathbf{x})) = \underset{(s,i)}{\operatorname{argmin}}(\|\mathbf{x}_{\text{RP},i_{\text{IS}},c,i}(s) - \mathbf{x}\|^2) \quad (1)$$

Another way is to choose a pathway with a low activation barrier among those that satisfy the IS structure and the condition c using Equation 2 and Equation 3. In the present experiment, we chose the paths in this way. Another option is to choose the pathway according to the Boltzmann distribution depending on the activation energy.

$$\hat{i}(i_{\text{IS}}, c, \mathbf{x}) = \underset{i}{\operatorname{argmin}} \left(\max_s (E(\mathbf{x}_{\text{RP},i_{\text{IS}},c,i}(s))) \right) \quad (2)$$

$$\hat{s}(i_{\text{IS}}, c, \mathbf{x}) = \underset{s}{\operatorname{argmin}} \left(\|\mathbf{x}_{\text{RP},i_{\text{IS}},c,\hat{i}(i_{\text{IS}},c,\mathbf{x})}(s) - \mathbf{x}\|^2 \right) \quad (3)$$

The direction of the tangent line along this reaction path is written with a red arrow in the Figure 1, \mathbf{t}_{tan} . \mathbf{t}_{tan} is defined as Equation 4

$$\mathbf{t}_{\text{tan}}(\mathbf{x}, \mathbf{x}_{\text{IS}}, c) = \left. \frac{d}{ds} \mathbf{x}_{\text{RP},i_{\text{IS}},c,\hat{i}(s)} \right|_{s=\hat{s}(i_{\text{IS}},c,\mathbf{x}),i=\hat{i}(i_{\text{IS}},c,\mathbf{x})} \quad (4)$$

The black arrow in the figure is a line connecting the point to the nearest point of the nearest reaction path, \mathbf{t}_{prp} . \mathbf{t}_{prp} is defined as Equation 5.

$$\mathbf{t}_{\text{prp}}(\mathbf{x}, \mathbf{x}_{\text{IS}}, c) = \mathbf{x}_{\text{RP}, i_{\text{IS}}, c, i}(s) \Big|_{s=\hat{s}(i_{\text{IS}}, c, \mathbf{x}), i=\hat{i}(i_{\text{IS}}, c, \mathbf{x})} - \mathbf{x} \quad (5)$$

Furthermore, we define t_{fin} as a variable that determines whether the reaction path is finished or not. The reaction path is a curve with finite length connecting IS and FS. Therefore, \mathbf{t}_{prp} is a line connecting current position and the end of the reaction path (IS or FS), or a perpendicular line to the reaction path. If \mathbf{t}_{prp} is a perpendicular line, $t_{\text{fin}} = 0$, and if the line connects current position and FS, $t_{\text{fin}} = 1$. \mathbf{t}_{tan} , \mathbf{t}_{prp} and t_{fin} were used for learning. The learning method is a slightly extended version of the same method as in the score matching [11] or flow matching [12], using the Equation 6 and Equation 7. where $y_{\text{std}, \text{tan}}$ and $y_{\text{std}, \text{prp}}$ are the predicted values of standard deviation by the neural network. By adding the standard deviation to the training, it is intended that the outputs do not need to be fitted to the inputs that are difficult to learn, and that the outputs can be further adjusted to the inputs that are easy to learn. Also, the equations 6 and 7 have the same form as the logarithm of the normal distribution. Let \mathbf{t}_{tan} be the learned output \mathbf{y}_{tan} . Let \mathbf{t}_{prp} be the learned output of \mathbf{y}_{prp} . Let \mathbf{y}_{fin} be the output of learning t_{fin} . The weighted sum of \mathbf{y}_{tan} and \mathbf{y}_{prp} is treated as the direction to go. In the experiment, we used weighted sum with weight=1 (Equation 9). \mathbf{y}_{fin} were used to decide whether to terminate the generation. The equation 8 was used to fit \mathbf{y}_{fin} .

$$l_{\text{tan}} = \frac{1}{2} \frac{\|\mathbf{y}_{\text{tan}}(\theta, \mathbf{x}, \mathbf{x}_{\text{IS}}, c) - \mathbf{t}_{\text{tan}}(\mathbf{x}, \mathbf{x}_{\text{IS}}, c)\|^2}{y_{\text{std}, \text{tan}}^2} + \log(y_{\text{std}, \text{tan}}^2(\theta, \mathbf{x}, \mathbf{x}_{\text{IS}}, c)) + \frac{3N}{2} \log(2\pi) \quad (6)$$

$$l_{\text{prp}} = \frac{1}{2} \frac{\|\mathbf{y}_{\text{prp}}(\theta, \mathbf{x}, \mathbf{x}_{\text{IS}}, c) - \mathbf{t}_{\text{prp}}(\mathbf{x}, \mathbf{x}_{\text{IS}}, c)\|^2}{y_{\text{std}, \text{prp}}^2} + \log(y_{\text{std}, \text{prp}}^2(\theta, \mathbf{x}, \mathbf{x}_{\text{IS}}, c)) + \frac{3N}{2} \log(2\pi) \quad (7)$$

$$l_{\text{fin}} = - \sum_{i_{\text{feat}}=0}^1 \log \frac{\exp([\mathbf{y}_{\text{fin}}(\theta, \mathbf{x}, \mathbf{x}_{\text{IS}}, c)]_{i_{\text{feat}}})}{\sum_{j_{\text{feat}}=0}^1 \exp([\mathbf{y}_{\text{fin}}(\theta, \mathbf{x}, \mathbf{x}_{\text{IS}}, c)]_{j_{\text{feat}}})} 1_{i_{\text{feat}}=t_{\text{fin}}} \quad (8)$$

$$\mathbf{y} = \mathbf{y}_{\text{prp}} + \mathbf{y}_{\text{tan}} \quad (9)$$

2.2 Relationship between flow matching

The model used in this study was greatly influenced by flow matching, diffusion mode, and reinforcement learning, and many changes were made. In ordinal diffusion models and flow matching, the concept of ‘‘time’’ is used to smoothly connect simple distributions and distributions to be generated. For example, $t = 0$ is a Gaussian distribution and $t = 1$ is the Boltzmann distribution that the numerator follows. In this sense, the proposed method can be interpreted as eliminating the concept of time since it does not require a simple distribution. On the other hand, it can be interpreted that a localized distribution around IS is used instead of a simple distribution, and a localized distribution around FS is used as the distribution to be generated. The difference in the latter interpretation is as follows. First, in the flow matching and diffusion models, the pathway itself is not important during the generation process, but only the distribution of the final state is important. In contrast, in the proposed method, the pathway itself is also important, and all the structures obtained during the generation process are used to construct the reaction pathway. In addition, the vector fields (without time) are learned in this problem setup, which is in contrast to the diffusion model and flow matching where the learned vector fields change with each time. The transition path from the IS along the learned vector field will be the reaction path. Since the vector field without time is used as the target of prediction, the number of steps to complete the generation is not uniquely determined, unlike general flow matching and diffusion models. Therefore, stopping condition were also predicted.

3 Experiments

3.1 Notation

The \otimes denote e3nn tensor products [13]. \oplus denotes a concatenate. The \odot denotes the operation of taking the product of two features and summing them in the feature direction. Symbols with a

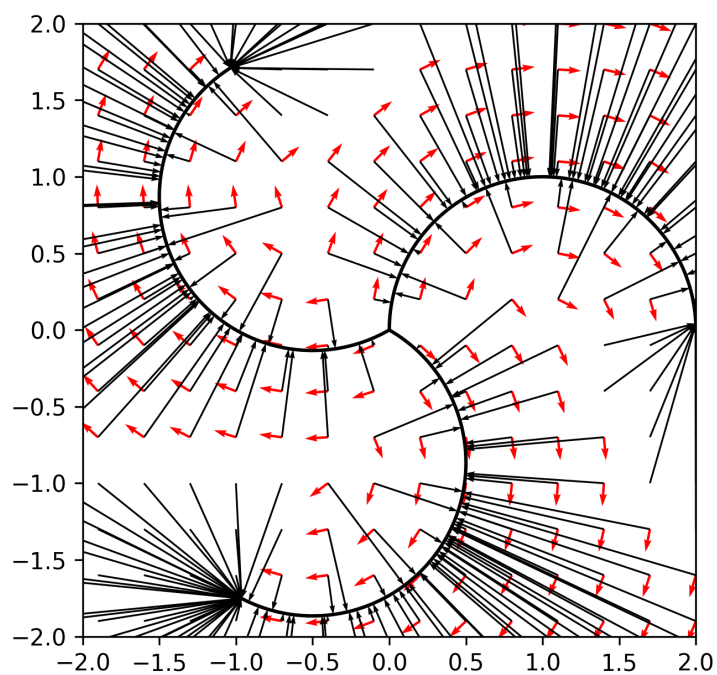


Figure 1: An image of the flow that has been learned. In the center of the figure, think of the IS. The three curves that come out from the IS are considered optimized reaction paths. The end of the reaction path that is not the IS are the FSs. The black arrows extending from each point in the whole figure are \mathbf{t}_{prp} , and the red arrows are \mathbf{t}_{prp} .

single index like Z_i indicate that the symbols are for the i th node (i th atom). Symbol with two indices like c_{ij} indicate that the symbols are for the edge between the i -th node and the j -th node. Also, values written in bold like \mathbf{r} are $E(3)$ -equivariant quantities. The $\hat{\mathbf{r}}$ denotes the normalized \mathbf{r} and $\|\mathbf{r}\|$ denotes the norm of \mathbf{r} . All variables are written in e3nn notation according to the transformation rules to which they belong. As a particularly important supplement, the $0e$ component is a $E(3)$ -invariant scalar component and the $1o$ component is an $E(3)$ -rotation equivariant vector component. In addition, when written as $128 \times 0e$, it indicates that the feature consists of 128 $E(3)$ -invariant scalar components. ‘‘FNN’’ denotes the operation of applying fully connected neural network with respect to the $0e$ component for each atom. The silu [14] activation functions were used. Resblock [15] was used for the transformations with the same number of inputs and outputs.

3.2 Neural network architecture

Let i and j be atomic indices. The overall architecture of the model is shown below. The formal input of the model is shown in Equation 10. where \mathbf{x}_i are the coordinates of the current structure and $\mathbf{x}_{\text{IS},i}$ are the coordinates of IS. Z_i is the atomic number. In addition, c_{ij} is a feature vector to specify the reaction to be generated. In this experiment, c deals only with edge features.

$$f_{\text{cart}} : \{\mathbf{x}_i, \mathbf{x}_{\text{IS},i}, Z_i, c_{ij}\} \longrightarrow \{\mathbf{y}_{\text{tan},i}, \mathbf{y}_{\text{prp},i}, y_{\text{std},i}, y_{\text{fin}}\} \quad (10)$$

In order to guarantee translation-rotation equivalence, only relative coordinates were used. The input/output using relative coordinates is shown in Figure 2 and Equation 11. where \mathbf{r} is the relative coordinate between atoms. There were 3 types of relative coordinates: 1. the relative coordinate $\mathbf{x}_{\text{IS},i} - \mathbf{x}_{\text{IS},j}$ between atoms in the IS structure, 2. the relative coordinate $\mathbf{x}_i - \mathbf{x}_j$ between atoms in the current structure, the relative coordinates $\mathbf{x}_i - \mathbf{x}_{\text{IS},i}$ between atoms in the IS and the current structure. They are collectively denoted as \mathbf{r}_{ij} . For the part of $\mathbf{x}_i - \mathbf{x}_{\text{IS},i}$, we adopt unidirectional edges.

$$f_{\text{rel}} : \{\mathbf{r}_{ij}, Z_i, c_{ij}\} \longrightarrow \{\mathbf{y}_{\text{tan},i}, \mathbf{y}_{\text{prp},i}, y_{\text{std},i}, y_{\text{fin}}\} \quad (11)$$

The pairing of (i, j) is based on Big Bird [16]. Big Bird is a method to make the edge of attention sparse in Transformer. In Big Bird, super nodes are prepared in addition to normal nodes. The edge is connected between nodes that are close to each other, between all nodes and the super node, and between randomly selected pairs of nodes. These three types of connections are called window, global, and random. In the present experiment, atoms within a distance of 12\AA were connected by selecting their closest neighbors up to 128th (window). In addition, 32 atoms were randomly connected from among the atoms within 30\AA (random). In addition, two supernodes were established and connected between the supernode and all atoms (global). Since supernodes do not have coordinates, the relative coordinates of the edges between supernodes are set to $\mathbf{r}_{ij} = \mathbf{0}$.

In Equation 11, $c_{ij} \in \{0, 1\}^9$ consists of 0 or 1 values that may or may not satisfy the conditions. The first condition indicates whether the reaction breaks the bond (i.e., the atoms are move far together). The second condition indicates whether the reaction forms a bond (i.e., whether the atoms move closer together). The third condition indicates whether the reaction rotates the dihedral angle around the bond by more than 105° . The third condition was set to zero if the first or second condition is satisfied. The fourth condition indicates whether the first three conditions are used as model inputs. When the fourth condition is set to 0, first to third conditions were set to 0. The fourth condition was set to 1 for conditional generation and 0 for unconditional generation. The fifth condition indicates whether the edge is an edge connecting the IS and the current structure for each interatomic bond. The sixth condition indicates whether the edge is a window connection. The seventh condition indicates whether the edge is a random connection. The eighth condition indicates whether this connection is an atom-supernode connection. The ninth condition indicates whether the connection is a supernode-supernode connection.

Figure 2 shows the whole model. One-hot vectors are used for embedding Z_i . The embedding of Z_i is further transformed by neural net nodewise, normalized, and treated as node features with only $0e$ component, which is the input of the first interaction block. The relative coordinate \mathbf{r}_{ij} is divided into relative distance $\|\mathbf{r}_{ij}\|$ and normalized relative coordinate $\hat{\mathbf{r}}_{ij}$ and embedded respectively. For embedding $\|\mathbf{r}_{ij}\|$, sinusoidal embedding [17] is used. For embedding $\hat{\mathbf{r}}_{ij}$, the spherical harmonic function of e3nn [13] where used. where the $1 \times 0e$ component is always 1 and the $1 \times 1o$ component is the normalized $\hat{\mathbf{r}}_{ij}$.

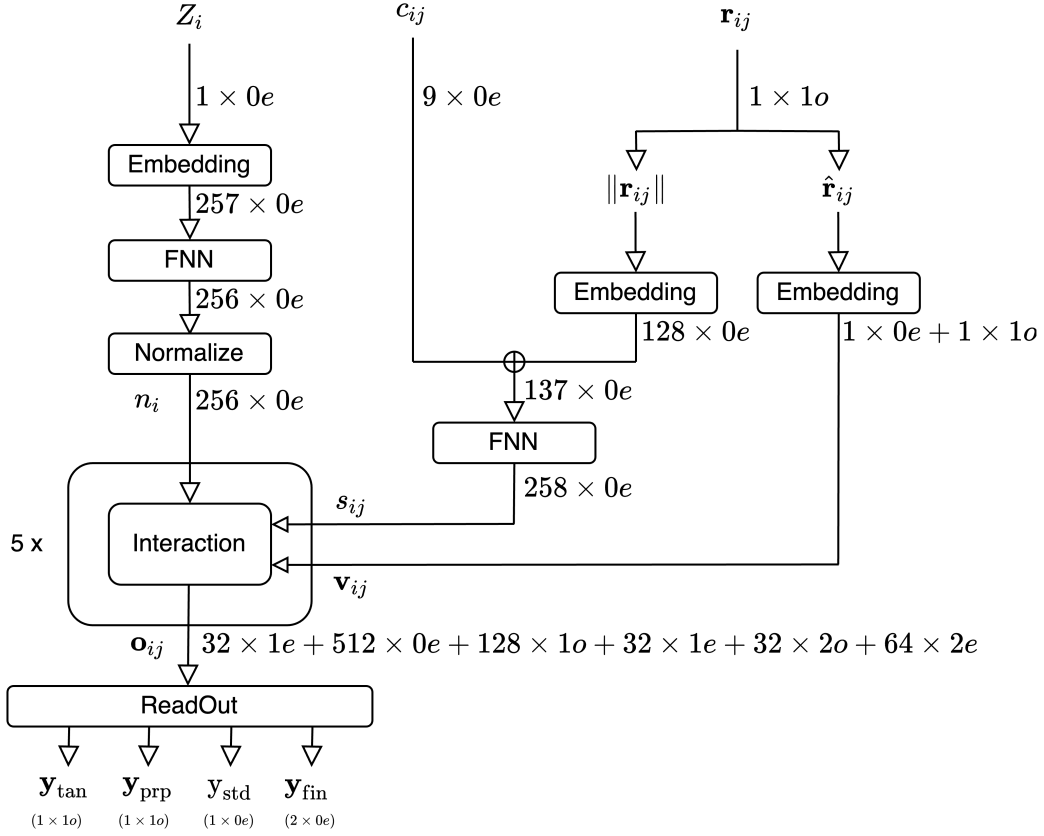


Figure 2: The whole model architecture used.

The embedding relative distance is a scalar feature for edges and satisfies the same transformation rule ($E(3)$ invariant) as c_{ij} . For this reason, it was concatenated with c_{ij} and treated as a node scalar feature. After concatenation, the result transformed by FNN is treated as input for the interaction block as the edge scalar feature S_{ij} . The embedding of the normalized relative coordinates was treated as input for the interaction block as the edge vector feature \mathbf{v}_{ij} .

The interactions are performed five times, during which S_{ij} and \mathbf{v}_{ij} are fixed. On the other hand, the node features have different values each time. In addition, since the tensor product of the node features and \mathbf{v}_{ij} is included inside the interaction block, the node features obtain higher-order tensor features at each interaction.

3.3 Interaction

The interaction part in Figure 2 is described in Figure 3 (a). An $E(3)$ -attention were implemented. Three edge features (\mathbf{q}_{ij} , \mathbf{k}_{ij} , \mathbf{v}_{ij}) were created using three edge feat blocks introduced in section 3.4. The single node feature \mathbf{n}_i is obtained from \mathbf{q}_{ij} , \mathbf{k}_{ij} , \mathbf{v}_{ij} by attention. Attention is represented by the Equations 12 and 13. In Equation 12, “ \cdot ” represents the inner product, which is the operation of adding the features after multiplying them all together. As a result, w_{ij} is $1 \times 0e$.

$$w_{ij} = \frac{\mathbf{q}_{ij} \cdot \mathbf{k}_{ij}}{\sqrt{d}} \quad (12)$$

$$\mathbf{n}'_i = \sum_j \left(\frac{\exp(w_{ij})}{\sum_k \exp(w_{ik})} \mathbf{v}_{ij} \right) \quad (13)$$

The \mathbf{n}'_i obtained by the Equation 13 is added to the \mathbf{n}_i of the input of the interaction block, and then normalized to obtain the overall output. Here, normalize is represented by the Equation 14. The

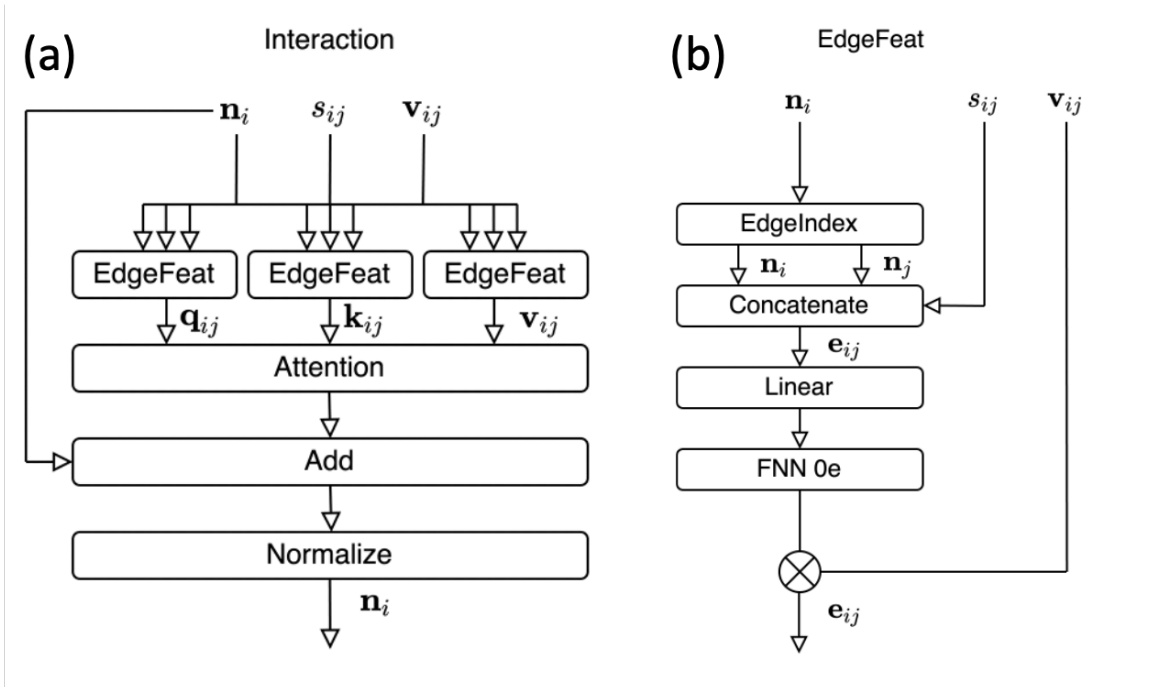


Figure 3: Diagrams of the interaction of the e3-attention network. (a) The whole diagram. (b) Details of the EdgeFeat block used in (a).

normalization in this method preserves rotational equivalence.

$$\frac{\mathbf{n}_i}{\sqrt{\mathbf{n}_i \cdot \mathbf{n}_i}} \quad (14)$$

3.4 EdgeFeat

In Section 3.3, we construct edge features with edge feat block. The edge feat block is described in the Figure 3(b). First, to represent the interaction, node features are represented as \mathbf{n}_i and \mathbf{n}_j . \mathbf{n}_i , \mathbf{n}_j , and s_{ij} were concatenated into single edge tensor feature. $O(3)$ linear transformation were performed, and FNN were applied. The result was used as a input for the tensor product with the edge vector feature to create output. This tensor product makes the features include components with higher ranks.

3.5 ReadOut

The readout part that exists in the Figure 2 is described in the Figure 4. There are four outputs. The output y_{fin} indicates the stopping condition and has a size of $2 \times 0e$. The output $y_{\text{std},i}$ is an output to allow for different prediction uncertainties for each atom, and has a size of $1 \times 0e$. The outputs $\mathbf{y}_{\text{tan},i}$ and $\mathbf{y}_{\text{prp},i}$ are the outputs for direction prediction. They have magnitude $1 \times 0o$ respectively. The inner product decoding (Section 3.6) was used to obtain the magnitudes of $\mathbf{y}_{\text{tan},i}$ and $\mathbf{y}_{\text{prp},i}$. The inner product decoding was also used for the orientation of $\mathbf{y}_{\text{tan},i}$ and $\mathbf{y}_{\text{prp},i}$, but the $1o$ component of the feature were used instead of the constant array. To obtain y_{fin} , the $0e$ features for all atoms were transformed by NN and the logsumexp is applied to aggregate the atomwise feature into molecular feature. The molecular feature was transformed by FNN to obtain y_{fin} .

3.6 Inner product decoding

The norm of the prediction vectors \mathbf{y}_{prp} and \mathbf{y}_{tan} , and the scalar value y_{std} , which indicates the certainty of the prediction, were decoded using inner product. After FNN transformation of the $0e$ component of the features, softmax was applied for the feature, and then inner product was performed with an array of equally spaced numbers of the same dimension as the feature. The arrays used to

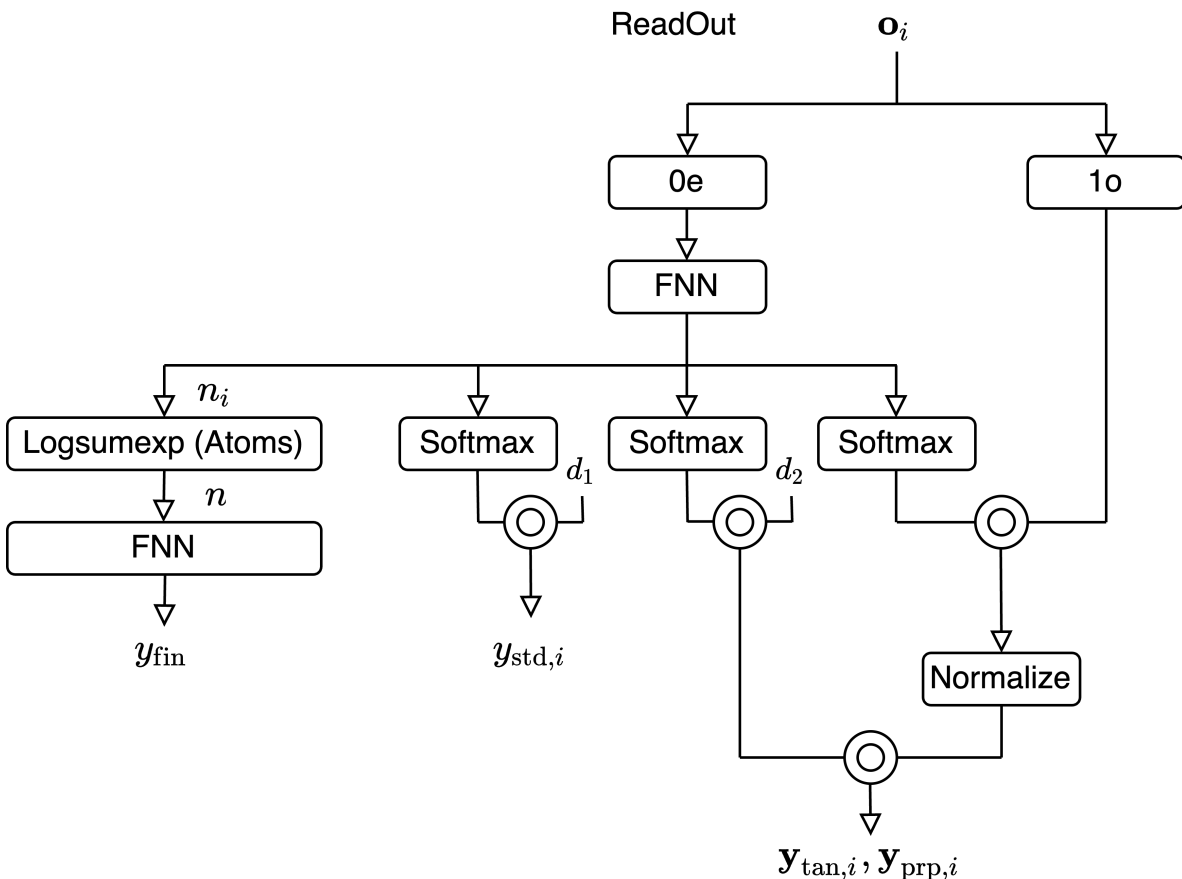


Figure 4: The readout block of the model architecture.

predict the norm of \mathbf{y}_{prp} and \mathbf{y}_{tan} are equally spaced arrays ranging from -2 \AA to 2 \AA in increments of 0.1 \AA . Sequences for predicting y_{std} are equally spaced from 0.1 \AA to 1.0 \AA in 0.1 \AA increments.

3.7 Dataset

Transition1x was used. The data set used was the data obtained by re-optimizing the reaction pathways of Transition1x with PFP v4. Some of the pathways were divided into multiple pathways by the re-optimization, and 10074 pathways were used. Among the IS and FS of these pathways, molecules whose energy difference is within 0.05 eV and the distance between the most migrated atoms is within 0.1 \AA are judged to be identical to each other. Only those reactions that involve bond changes or rotations of dihedral angles are extracted, and only those reactions that have the lowest activation barriers among the reactions sharing the same IS and FS are also extracted. While this process remove some pathways, all pathways are duplicated twice in round-trip. As a result, 11801 reactions are treated as unique pathways. Next, the dataset were divided into train, valid, and test datasets. Molecules with the same composition were divided into the same group. Therefore, it is guaranteed that there is no identical data in train and valid. Of the total composition, 90% was treated as train data. 5% was treated as validation data. The remaining 5% were treated as test data.

3.8 sampling

The coordinates of the data used in the flow matching were sampled along the RPs. One reaction path is selected, the structure with noise on IS is set as the initial value, and the data is sampled by moving in the direction of the reaction path, approaching the reaction path, and adding noise on it as in Equation 15. where dw is a wiener process. g was sampled uniformly from the range $[0.0, 0.2]$ each

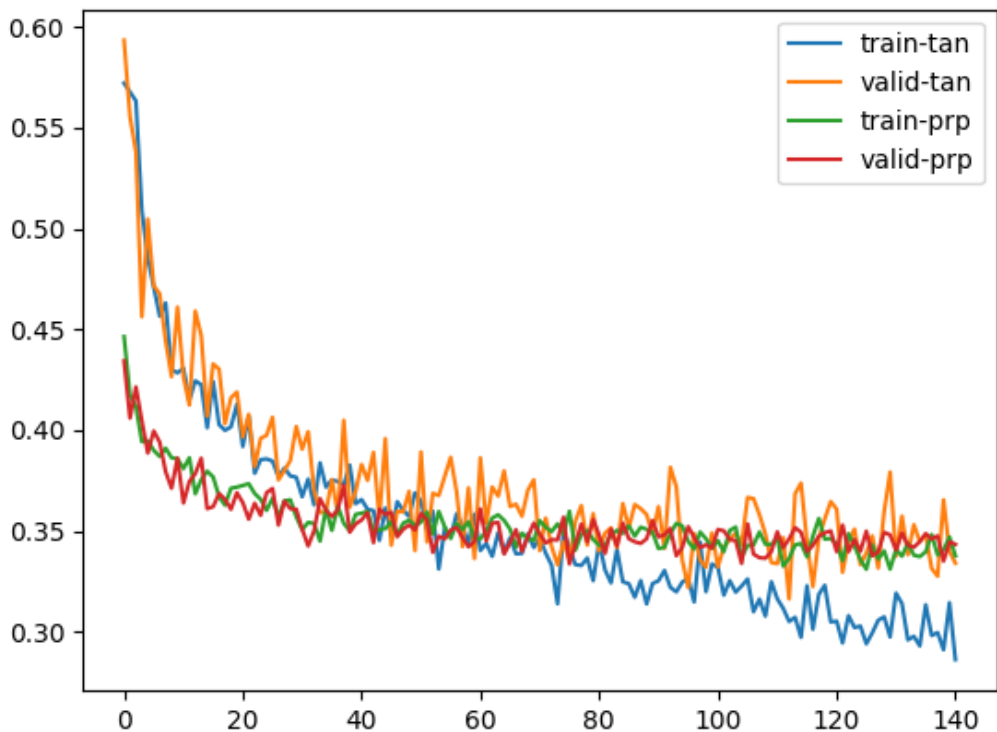


Figure 5: The learning curve when trained on transition1x.

time the reaction path was selected. This process samples the structure around the reaction path.

$$dx = (\mathbf{t}_{\text{tan}} + \mathbf{t}_{\text{prp}})dt + gdw \quad (15)$$

The obtained distribution is tubular around the reaction path. In order to facilitate the learning of t_{fin} , the ratio of data used was selected to the ratio between $t_{\text{fin}} = 0$ and $t_{\text{fin}} = 1$ become 1:1. In order to also learn unconditional generation, training with unconditional generation was performed with a probability of 0.3 and conditional generation was performed with a probability of 0.7.

4 Result

4.1 training

The learning curve is shown in Figure 5. While the training loss for \mathbf{y}_{prp} immediately stopped with a few steps, the training loss for \mathbf{y}_{tan} continued to decrease. In the latter half of the period, the training loss for \mathbf{y}_{tan} continues to decrease, while the validation loss stopped decreasing in the middle of the period.

4.2 Generation examples

Examples of the results of conditional generation with changes in bonds are shown in Figure 6. Classifier free guidance, described in Section 4.3, with $w = 4$ were performed for C8H9O reaction from yarp reaction dataset [18]. Even though the transition1x data set, which is used for training, contains only up to C7, we were able to generate the reaction in the molecules shown in the figure, which is C8H9O. The first reaction in Figure 6 includes the rotation of dihedral angles and the formation of bonds, and to create the initial values of such reaction pathways without a neural network requires detailed

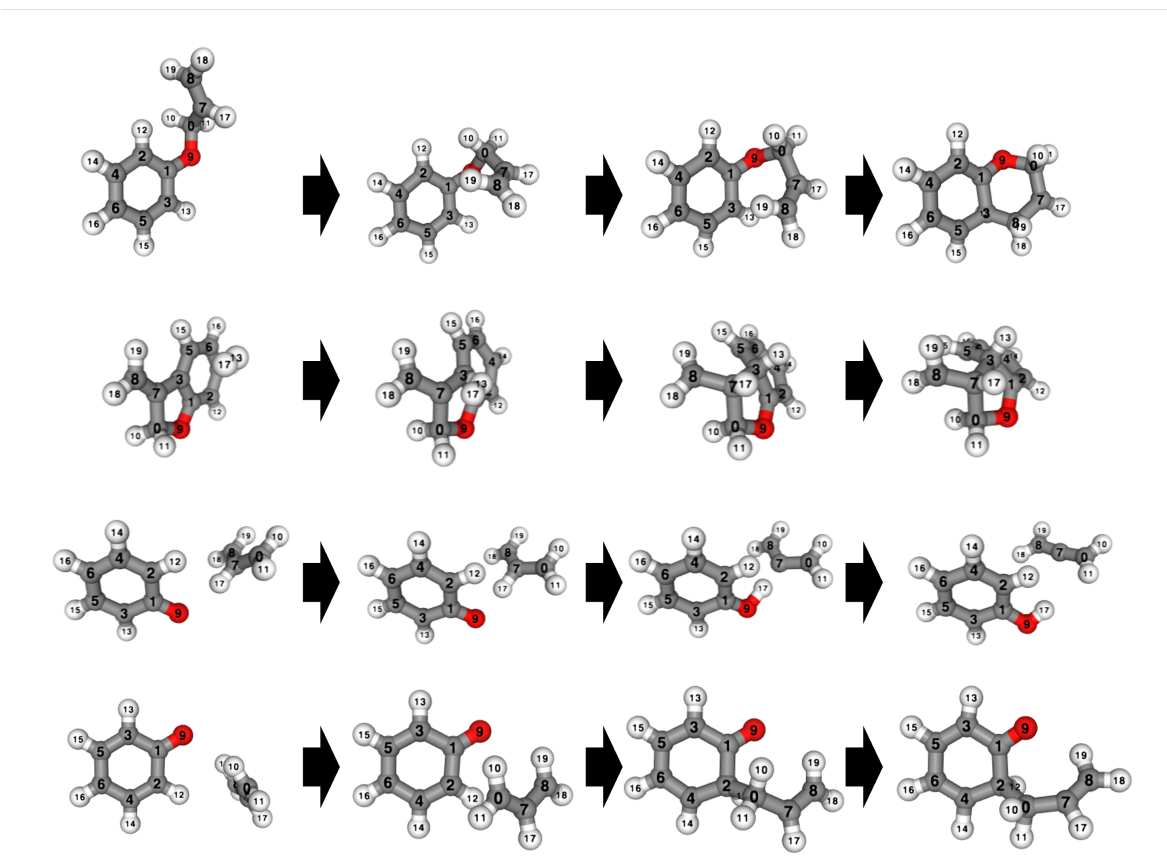


Figure 6: Conditional generation results for C8H9O. Top: determines c to combine 3 and 8. Second: combines 7 and 17, 0 and 11, and dissociate 17 and 11. Third: combine 17 and 7, and 17 and 9. Fourth combine 0 and 2.

manipulations of the dihedral rotation and bond formation, which is a very labor-intensive task. By using this neural network, this reaction can be created in a few tens of seconds, only by specifying the formation of the bond. In addition, the first reaction of Figure 6 includes a dihedral rotation, and the reaction coordinates are greatly bent from the cartesian coordinates, but nevertheless, the model were able to give a qualitatively correct reaction path. Other reaction in the Figure 6 have a lot of kind of the reactions. The second reaction is a hydrogen addition reaction to a double bond. The third reaction is a hydrogen transfer reaction. The fourth reaction is a binding of two molecules.

4.3 Conditional generation

Conditional generations were performed on the 833 test data by changing the coupling. For the conditional generation, we used classifier free guidance [19]. The equation used is also shown in the Equation 16.

$$\mathbf{y}(\theta, \mathbf{x}, \mathbf{x}_{\text{IS}}, c, w) = (1 + w)\mathbf{y}(\theta, \mathbf{x}, \mathbf{x}_{\text{IS}}, c) - w\mathbf{y}(\theta, \mathbf{x}, \mathbf{x}_{\text{IS}}, 0) \quad (16)$$

The larger the value of w , the more the reactions proceeded satisfying the given conditions for more data. The results are shown in Table 1. Among the results obtained by the classifier free guidance with $w = 8.0$, those that satisfy the given conditions are optimized with the PFP v4.0.0 level using the string method, and the activation barriers of the corresponding data in the test data set were compared. In this comparison, it is expected that the same activation barriers were obtained if the outputs are qualitatively the same paths. The results are shown in Figure 7 (a). And the histogram for the energy difference between generated-optimized RP and test RP is shown in Figure 7 (b). Most reactions exhibited the same activation barriers as in the test data set and would be expected to have followed qualitatively similar pathways. On the other hand, some reactions followed very different pathways from the test data set and gave qualitatively different activation barriers. transition1x is a

w	number	ratio
0.0	519	0.62
0.5	662	0.79
1.0	714	0.85
2.0	753	0.90
4.0	785	0.94
8.0	790	0.95

Table 1: w is a parameter of classifier free guidance. number is the number of reaction pathways whose results satisfy the generation conditions. ratio is the number of successful pathways divided by the number of test data.

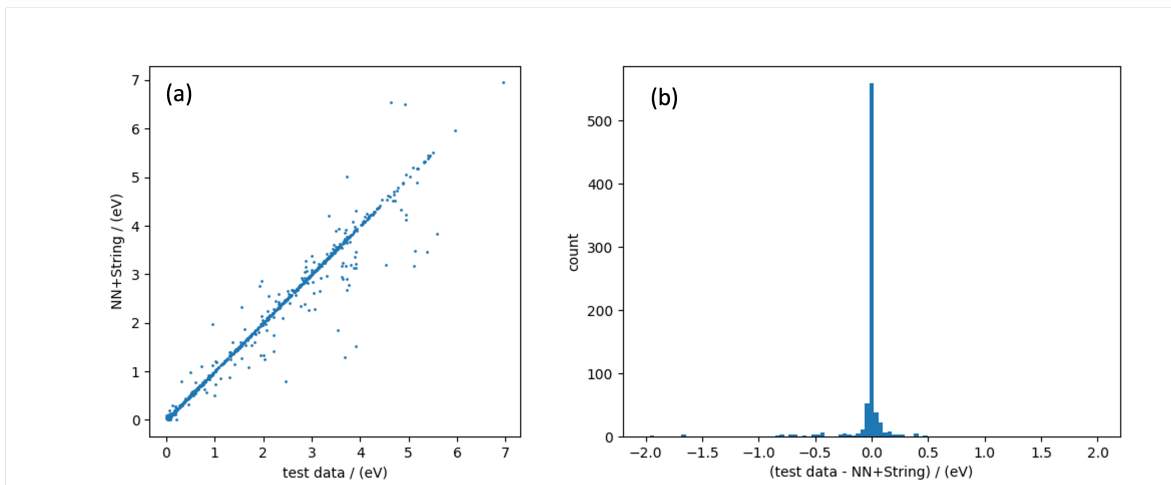


Figure 7: (a) Comparison of activation barriers for reactions in test data set vs. activation barriers for generated-optimized results. (b) The histogram for energy difference between test data and generated-optimized RP.

data set that contains a variety of reactions, so it is difficult to generate exactly the same reactions as in the test data. The current experiment sometimes gave reactions with higher activation barriers than the test data, but rather sometimes gave pathways with lower barriers than the test data. Future development is needed in this regard with respect to data set expansion and data selection rather than model accuracy.

4.4 Random generation

White noise was added during the generation process. The Equation 17 was used for generation. Reaction pathways were randomly generated 16 times each from the ISs in the Test dataset and analyzed for changes in bonds and rotations between the structural optimized ISs and FSs. The number of reactions that gave different changes generated from each IS was counted. Here, the number 16 is an artificial cutoff. Because of the large number of test datasets, each dataset was generated only 16 times to reduce the computational cost of the experiment.

$$d\mathbf{x} = (\mathbf{y}_{\text{prp}} + \mathbf{y}_{\text{tan}})dt + g d\mathbf{w} \quad (17)$$

0.1 was used for dt and 0.1 was used for g . A histogram of the results is shown in Figure 8. Some ISs produced the same reaction each time, but often produced different reactions.

5 Conclusion

A machine learning model for reaction path generation was proposed. The model can be used to obtain a rough sketch of the entire reaction pathway with a small number of Neural Network evaluations.

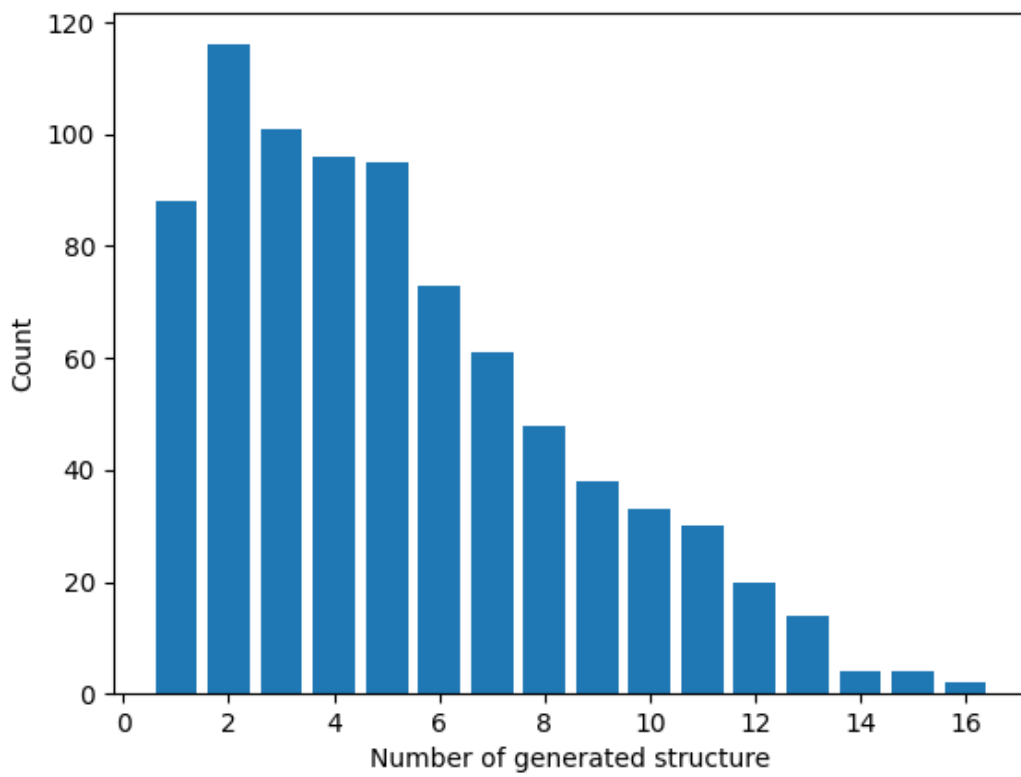


Figure 8: Histogram of the number of occurrences of the FS structure generated by 16 random generation runs from each IS.

The model can handle reaction pathways in 3N-dimensional space and can generate complex reactions such as organic reactions. The model was able to learn and generalize the transition1x results to generate reactions similar to the test data. The model could be used for both conditional and random generation. In this experiment, conditional generation was performed using changes in bonding. With proper use of classifier-free guidance, response paths were generated that well reproduced the bond changes in the test data. In addition, when randomness were included in the generation, many types of reactions were generated from each initial state.

References

- [1] Henkelman, G.; Uberuaga, B. P.; Jónsson, H. A climbing image nudged elastic band method for finding saddle points and minimum energy paths. *J. Chem. Phys.* **2000**, *113*, 9901–9904.
- [2] Zimmerman, P. Reliable Transition State Searches Integrated with the Growing String Method. *J. Chem. Theory Comput.* **2013**, *9*, 3043–3050.
- [3] Garcia Satorras, V.; Hoogeboom, E.; Fuchs, F.; Posner, I.; Welling, M. E (n) equivariant normalizing flows. *Adv. Neural Inf. Process. Syst.* **2021**, *34*, 4181–4192.
- [4] Corso, G.; Stärk, H.; Jing, B.; Barzilay, R.; Jaakkola, T. DiffDock: Diffusion Steps, Twists, and Turns for Molecular Docking. **2022**,
- [5] Klein, L.; Krämer, A.; Noé, F. Equivariant flow matching. **2023**,
- [6] Zheng, S. et al. Towards Predicting Equilibrium Distributions for Molecular Systems with Deep Learning. **2023**,
- [7] Triplett, L.; Lu, J. Diffusion Methods for Generating Transition Paths. **2023**,
- [8] Sickafus, K. E.; Kotomin, E. A.; Uberuaga, B. P. *Radiation Effects in Solids*; Springer Science & Business Media, 2007.
- [9] Tang, H.; Li, B.; Song, Y.; Liu, M.; Xu, H.; Wang, G.; Chung, H.; Li, J. Reinforcement learning-guided long-timescale simulation of hydrogen transport in metals. **2023**,
- [10] Schreiner, M.; Bhowmik, A.; Vegge, T.; Busk, J.; Winther, O. Transition1x - a dataset for building generalizable reactive machine learning potentials. *Sci Data* **2022**, *9*, 779.
- [11] Ho, J.; Jain, A.; Abbeel, P. Denoising diffusion probabilistic models. *Adv. Neural Inf. Process. Syst.* **2020**, *33*, 6840–6851.
- [12] Lipman, Y.; Chen, R. T. Q.; Ben-Hamu, H.; Nickel, M.; Le, M. Flow Matching for Generative Modeling. **2022**,
- [13] Geiger, M.; Smidt, T. e3nn: Euclidean Neural Networks. **2022**,
- [14] Hendrycks, D.; Gimpel, K. Gaussian Error Linear Units (GELUs). **2016**,
- [15] He, K.; Zhang, X.; Ren, S.; Sun, J. Deep residual learning for image recognition. Proceedings of the IEEE conference on computer vision and pattern recognition. 2016; pp 770–778.
- [16] Zaheer, M.; Guruganesh, G.; Dubey, A.; Ainslie, J.; Alberti, C.; Ontanon, S.; Pham, P.; Ravula, A.; Wang, Q.; Yang, L.; Ahmed, A. Big Bird: Transformers for Longer Sequences. **2020**,
- [17] Vaswani, A.; Shazeer, N.; Parmar, N.; Uszkoreit, J.; Jones, L.; Gomez, A. N.; Kaiser, L.; Polosukhin, I. Attention is all you need. *Adv. Neural Inf. Process. Syst.* **2017**, *30*.
- [18] Zhao, Q. YARP reaction database. figshare. Dataset, 2021; <https://doi.org/10.6084/m9.figshare.14766624.v7>.
- [19] Ho, J.; Salimans, T. Classifier-Free Diffusion Guidance. **2022**,